



# The impact of volcanic aerosol on the Northern Hemisphere stratospheric polar vortex: mechanisms and sensitivity to forcing structure

M. Toohey<sup>1</sup>, K. Krüger<sup>1,2</sup>, M. Bittner<sup>3,4</sup>, C. Timmreck<sup>3</sup>, and H. Schmidt<sup>3</sup>

<sup>1</sup>GEOMAR Helmholtz Centre for Ocean Research Kiel, Kiel, Germany

<sup>2</sup>University of Oslo, Department of Geosciences, Oslo, Norway

<sup>3</sup>Max Planck Institute for Meteorology, Hamburg, Germany

<sup>4</sup>International Max Planck Research School on Earth System Modeling (IMPRS), Hamburg, Germany

Correspondence to: M. Toohey (mtoohey@geomar.de)

Received: 9 May 2014 – Published in Atmos. Chem. Phys. Discuss.: 25 June 2014

Revised: 29 October 2014 – Accepted: 3 November 2014 – Published: 9 December 2014

**Abstract.** Observations and simple theoretical arguments suggest that the Northern Hemisphere (NH) stratospheric polar vortex is stronger in winters following major volcanic eruptions. However, recent studies show that climate models forced by prescribed volcanic aerosol fields fail to reproduce this effect. We investigate the impact of volcanic aerosol forcing on stratospheric dynamics, including the strength of the NH polar vortex, in ensemble simulations with the Max Planck Institute Earth System Model. The model is forced by four different prescribed forcing sets representing the radiative properties of stratospheric aerosol following the 1991 eruption of Mt. Pinatubo: two forcing sets are based on observations, and are commonly used in climate model simulations, and two forcing sets are constructed based on coupled aerosol–climate model simulations. For all forcings, we find that simulated temperature and zonal wind anomalies in the NH high latitudes are not directly impacted by anomalous volcanic aerosol heating. Instead, high-latitude effects result from enhancements in stratospheric residual circulation, which in turn result, at least in part, from enhanced stratospheric wave activity. High-latitude effects are therefore much less robust than would be expected if they were the direct result of aerosol heating. Both observation-based forcing sets result in insignificant changes in vortex strength. For the model-based forcing sets, the vortex response is found to be sensitive to the structure of the forcing, with one forcing set leading to significant strengthening of the polar vortex in

rough agreement with observation-based expectations. Differences in the dynamical response to the forcing sets imply that reproducing the polar vortex responses to past eruptions, or predicting the response to future eruptions, depends on accurate representation of the space–time structure of the volcanic aerosol forcing.

## 1 Introduction

The Northern Hemisphere (NH) stratospheric winter polar vortex, which shows considerable interannual and intra-seasonal variability, has been observed to be stronger than normal in winters after major volcanic eruptions (Kodera, 1995; Labitzke and van Loon, 1989). While this observation is based on a relatively small sample (limited to the winters after the 1963 Agung, 1982 El Chichón and 1991 Pinatubo eruptions), the theoretical argument to explain such a strengthening appears clear: namely, that heating of the lower stratosphere through the absorption of radiation by volcanic sulfate aerosols enhances the equator-to-pole temperature gradient in the lower stratosphere, which, through the thermal wind equation, leads to stronger westerly winds (Robock, 2000 and references therein). Satellite observations clearly show a warming of the tropical lower stratosphere after volcanic eruptions (Labitzke and McCormick, 1992), so changes in meridional temperature gradients and zonal

winds are logical consequences. The degree to which secondary feedback mechanisms – such as changes in ozone or upward propagating planetary waves (e.g. Graf et al., 2007; Stenchikov et al., 2006) – also affect the vortex strength is at present unclear.

Post-volcanic strengthening of the NH polar vortex is an important step in a proposed mechanism which explains observed changes in surface climate in post-eruption winters (Kodera, 1994; Perlwitz and Graf, 1995). Specifically, it is thought that through stratosphere–troposphere coupling (Baldwin and Dunkerton, 2001; Gerber et al., 2012) the volcanically induced strong stratospheric polar vortex leads to the observed positive anomalies in surface dynamical indexes such as the Northern Annular Mode (NAM) or North Atlantic Oscillation (NAO) (Christiansen, 2008). Such dynamical changes lead to the “winter warming” pattern of post-volcanic temperature anomalies (Robock and Mao, 1992), which is characterized by warmer temperatures over large regions of the NH continents during winter which oppose the overall cooling impact of the volcanic aerosols on the surface. On the other hand, in a model study, Stenchikov (2002) found that a positive phase of the NAM was also produced in an experiment in which only the tropospheric impact of volcanic aerosols was included, implying that aerosol heating in the lower tropical stratosphere is not necessary to force a positive NAM response. Whatever the mechanisms, observations show that 11 out of 13 eruptions since 1870 were followed by positive wintertime NAO values (Christiansen, 2008): the apparent robustness of this post-eruption dynamical response should allow for enhanced skill in seasonal prediction for winters that follow volcanic eruptions (e.g. Marshall et al., 2009).

While a number of early model simulations reported qualified success in simulating the atmospheric dynamical response to volcanic eruptions (e.g. Graf et al., 1993; Kirchner et al., 1999; Rozanov, 2002; Shindell et al., 2001), assessments of the multi-model ensembles of the Coupled Model Intercomparison Projects (CMIP) 3 and 5 showed no significant winter warming response to prescribed volcanic forcing, nor did they show significant anomalies in post-eruption dynamical quantities in the stratosphere or at the surface (Driscoll et al., 2012; Stenchikov et al., 2006). It has been suggested that in order for a model to successfully respond to volcanic forcing, it should include a reasonably well-resolved stratosphere (Shindell, 2004; Stenchikov et al., 2006). However, analysis of the CMIP5 ensemble revealed no appreciable systematic difference in post-eruption geopotential height anomalies to volcanic aerosol forcing between models with or without well-resolved stratospheres (Charlton-Perez et al., 2013).

Most model simulations that incorporate the impact of volcanic eruptions, such as the CMIP3 and 5 historical simulations, do so using prescribed volcanic aerosol fields, which have associated uncertainties. In this study we investigate how the response of the atmosphere to volcanic aerosol forc-

ing depends on the prescribed aerosol forcing used in the simulation. We use one CMIP5 model, the MPI-ESM, and focus on the first winter after Mt. Pinatubo, the period of strongest volcanic forcing within the era of satellite observations. We run ensemble simulations using four different forcing data sets: two observation-based forcing sets, based primarily on different versions of SAGE II aerosol extinction measurements, and two model-constructed aerosol forcing sets. By assessing the model response to these forcing sets, we investigate (1) the mechanisms linking volcanic aerosol heating in the lower tropical stratosphere and NH winter vortex strength, (2) what stratospheric circulation responses to volcanic aerosol forcing are robustly produced by the model and forcings, and (3) the sensitivity of the vortex response to changes in the space–time structure of the volcanic forcing.

## 2 Experiment: observational basis, model and methods

In this section, the hypothesis that volcanic eruptions produce a strengthened NH winter polar vortex is briefly summarized by examining ERA-Interim reanalysis data. Then, the materials and methods of the present modelling study are presented including the model and volcanic forcing sets used, and the design of the ensemble simulations and analysis.

### 2.1 NH polar vortex response to volcanic eruptions in ERA-interim

The NH polar vortex is highly variable as a result of unforced internal variability, and the impact of external forcings such as volcanic eruptions, the 11 year solar cycle, the El Niño–Southern Oscillation (ENSO), and the Quasi Biennial Oscillation (QBO). Isolating the vortex response to any individual forcing term can be difficult, especially in the case of major volcanic eruptions for which so few actual events have occurred within the era of satellite measurements.

A common and simple method to isolate the pure volcanic impact on the state of the NH winter stratosphere is to simply average post-eruptive anomalies over winters after recent major volcanic eruptions. This technique is here applied to ERA-Interim reanalysis (Dee et al., 2011) temperature and zonal wind fields after the eruptions of El Chichón (1982) and Pinatubo (1991). Post-eruption winter anomalies are constructed for the two winters after each eruption by differencing post-eruptive December-to-February (DJF) mean fields with fields averaged for 3 (El Chichón) and 5 (Pinatubo) years before the eruption (the shorter reference period for El Chichón results from the fact that the ERA-Interim data set begins in 1979). Differences in post-eruption anomalies for Pinatubo are not strongly dependent on the choice of a 3, 4 or 5 year reference period.

Figure 1 (left) shows ERA-Interim temperature and zonal wind anomalies composited for four winters, the two winters each after Pinatubo and El Chichón. Mean tempera-

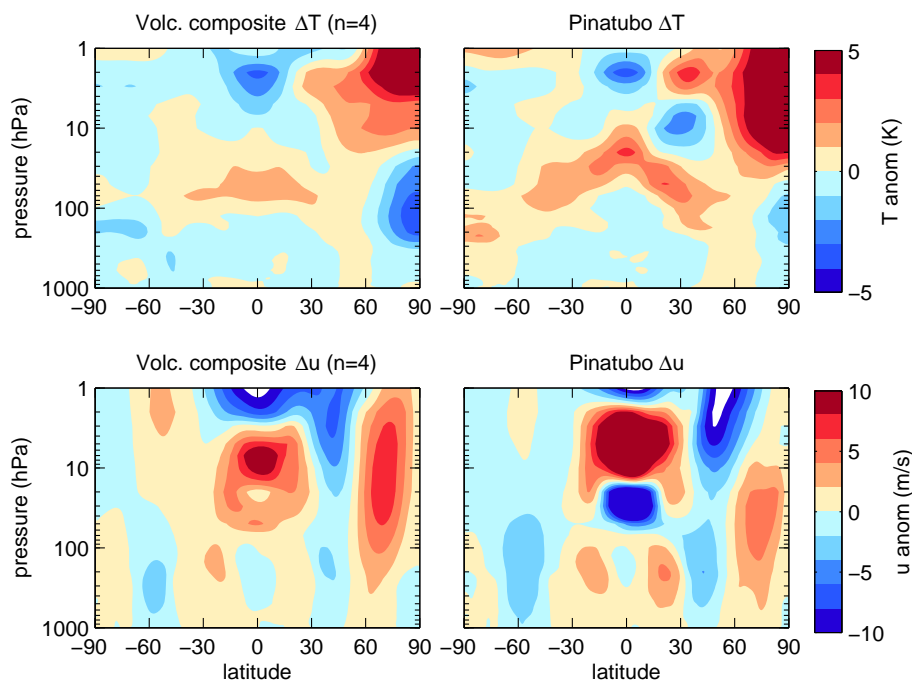


**Figure 1.** ERA-Interim DJF (top) temperature and (bottom) zonal wind anomalies for (left) post-volcanic composite ( $n = 4$ ) of two winters after eruptions of El Chichón and Pinatubo, and (right) 1991/92, the first winter after the Pinatubo eruption.

ture anomalies in the post-volcanic composite show positive anomalies in the tropical lower stratosphere, as would be expected due to aerosol heating. Temperature anomalies also show cooling of the tropical upper stratosphere, cooling of the NH polar lower stratosphere, and warming of the NH polar upper stratosphere. Mean post-volcanic zonal winds show a strengthening of the NH winter polar vortex by  $\sim 6 \text{ m s}^{-1}$ . Such a simple average with a small sample size does not completely remove the influences of variability resulting from other forcing terms – notably, the solar cycle was at a maximum at the times of both the El Chichón and Pinatubo eruptions, and El Niño events were observed in the first winters after both eruptions – but the composite temperature and zonal wind anomaly structure is certainly a better approximation of the direct volcanic impact than anomalies in any single post-volcanic year. For comparison, single winter anomalies are shown for the first winter after the Pinatubo eruption. Temperature anomalies for DJF 1991/92 roughly follow the structure of the 4 year composite, albeit with tropical positive anomalies located at higher altitudes, and weaker polar lower stratosphere cooling. Post-Pinatubo zonal wind anomalies in the tropics reflect the state of the QBO at the time, with negative (easterly) wind anomalies in the middle stratosphere ( $\sim 50\text{--}15 \text{ hPa}$ ) and positive (westerly) anomalies in the upper stratosphere ( $15\text{--}2 \text{ hPa}$ ). The polar vortex in the first post-Pinatubo winter was actually not as clearly enhanced as the 4 year composite, with positive zonal wind anomalies only in the mid to lower polar stratosphere centred at  $\sim 70^\circ \text{ N}$ . It is likely that in addition to the volcanic

forcing, the vortex in DJF 1991/92 was weakened somewhat due to the influences of the concurrent forcing of the El Niño and QBO easterly phase. Based on these arguments, it can be hypothesized that the pure response of the stratosphere to Pinatubo aerosol forcing would have the approximate structure of the composite response shown in Fig. 1 (left), albeit with greater amplitude, since the aerosol optical depth and hence aerosol radiative heating during the first post-Pinatubo winter is the strongest of the years used in the volcanic composite. This “expected” response in the first post-Pinatubo winter is based on a small sample size of observations, and an assumption of linear response to the magnitude of volcanic forcing; however, in light of limited evidence, it represents a best first-order, observation-based expectation, consistent with that assumed explicitly or implicitly in prior studies.

## 2.2 MPI-ESM

The MPI-ESM is a full Earth system model, with atmosphere, ocean, carbon cycle, and vegetation components. Major characteristics of the full ESM and its performance in the CMIP5 experiments are described by Giorgetta et al. (2013). The “low resolution” model configuration (MPI-ESM-LR) is used here, with horizontal resolution of the atmospheric component given by a triangular truncation at 63 wave numbers (T63) and 47 vertical layers extending to  $0.01 \text{ hPa}$ . Unlike model configurations with higher vertical resolutions, the LR version has no internally generated QBO.

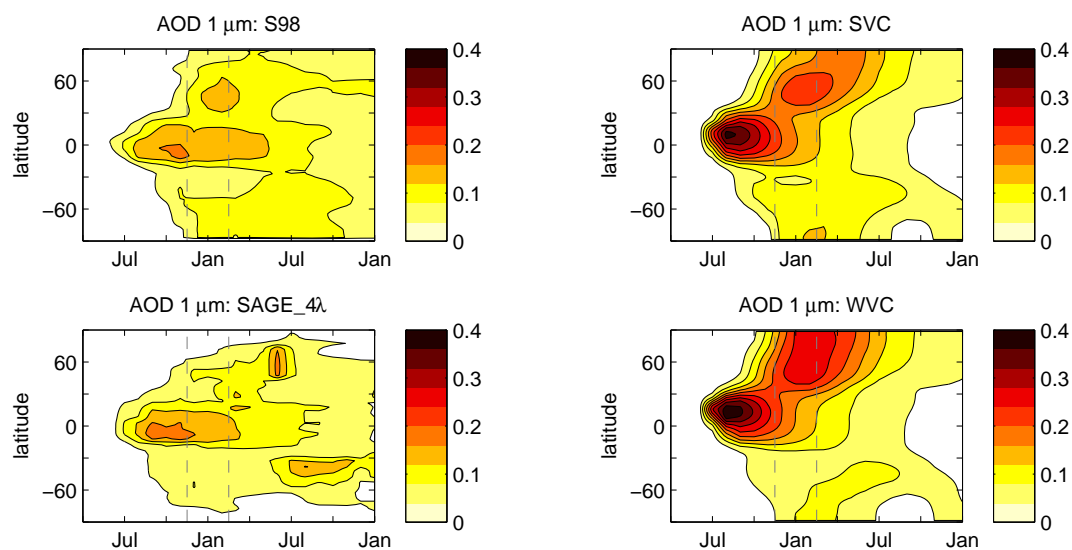


**Figure 2.** Zonal mean aerosol optical depth at  $1\ \mu\text{m}$  for the Pinatubo eruption, (left) as reconstructed from observations producing the S98 and SAGE\_4 $\lambda$  forcing data sets and (right) based on MAECHAM5-HAM model simulations and composited according to strong (SVC) and weak (WVC) vortex states. Dashed vertical lines demarcate the DJF period of interest.

CMIP5 historical simulations have previously been performed with the MPI-ESM over the time period 1850–2005. Prescribed external forcings for the historical simulations, including volcanic aerosols as well as greenhouse gases and ozone, follow CMIP5 recommendations, and the responses to these forcings are described by Schmidt et al. (2013).

The MPI-ESM is configured to take volcanic aerosol forcing data in two formats, both of which are used in this study. One format consists of monthly zonal mean values of aerosol extinction, single scattering albedo, and asymmetry factor as a function of time, pressure, and the 30 short wave and long wave spectral bands used by the model. This format is consistent with the observation-based forcings sets introduced in Sect. 2.3. A second format consists of monthly zonal mean aerosol extinction at  $0.55\ \mu\text{m}$ , and zonal mean effective radius, both as a function of latitude, height, and time. Pre-calculated look-up tables are then used to scale the  $0.55\ \mu\text{m}$  extinction to the wavelengths of the model's radiation code based on the effective radius. This methodology has been used to perform MPI-ESM simulations using the forcing time series of Crowley et al. (2008, e.g. Timmreck et al., 2009) or output from prior runs of the MAECHAM5-HAM coupled aerosol–climate model (e.g. Timmreck et al., 2010) as done in this study and described in Sect. 2.4.

### 2.3 Observation-based aerosol forcing sets

Volcanic sulfate aerosol forcing for the MPI-ESM CMIP5 historical simulations is based on an extended version of the aerosol data set developed by Stenchikov et al. (1998, hereafter S98) on the basis of SAGE II measurements of aerosol extinction at  $1.02\ \mu\text{m}$  and estimates of effective radii derived

from instruments on the Upper Atmosphere Research Satellite. The data are given at 40 pressure levels and interpolated to the actual hybrid model layers during the simulations. The S98 data set is based primarily on retrievals of aerosol extinction at  $1.02\ \mu\text{m}$  from SAGE II, with gaps filled with data from ground-based lidar systems. Together, the S98 forcing set and that from Sato et al. (1993, with updates <http://data.giss.nasa.gov/modelforce/strataer/>), both primarily based on SAGE II data, have been used in roughly half of the models that performed CMIP5 historical simulations (Driscoll et al., 2012).

Subsequent updates to the SAGE II retrievals have led to significant changes in the space–time morphology of the estimated aerosol extinction after Pinatubo (Arfeuille et al., 2013; Thomason and Peter, 2006). A new volcanic forcing set (SAGE\_4 $\lambda$  Arfeuille et al., 2013) has been compiled and made available to modelling centres ([http://www.pa.op.dlr.de/CCMI/CCMI\\_SimulationsForcings.html](http://www.pa.op.dlr.de/CCMI/CCMI_SimulationsForcings.html)), specifically for use in chemistry climate simulations within the Chemistry Climate Model Intercomparison (CCMI) initiative (Eyring and Lamarque, 2013). Time series of zonal mean aerosol optical depth (AOD) at  $1\ \mu\text{m}$  – the wavelength closest to the original SAGE II measurements and so less impacted by uncertainties in derived aerosol size distribution – are shown in Fig. 2 over the Pinatubo period for the S98 and SAGE\_4 $\lambda$  reconstructions.

It should be noted that even for Pinatubo – the best-observed eruption in history – the observation-based volcanic aerosol forcing sets suffer from significant but mostly unquantified uncertainties. Most notably, gaps in the satellite record result from sparse sampling of the satellite instruments (Stenchikov et al., 1998) and the fact that large optical

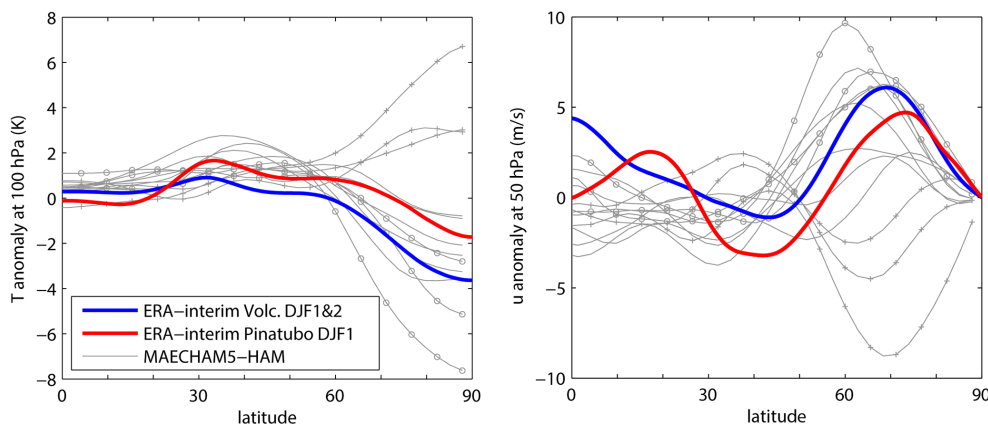


**Figure 3.** First post-eruption NH winter (DJF) anomalies of (left) temperature at 100 hPa and (right) zonal wind at 50 hPa for the 12-member MAECHAM5-HAM Pinatubo ensemble of Tooney et al. (2011) (grey lines). Ensemble members constituting the strong and weak vortex composites (SVC and WVC) as defined in the main text are marked by circles and crosses, respectively. For comparison, ERA-Interim anomalies based on a composite of the two winters after the eruptions of El Chichón and Pinatubo (blue), and the single winter after the Pinatubo eruption (red) are also shown.

depths in the initial months after the Pinatubo eruption reduced atmospheric transmission below detectability (Russell et al., 1996).

## 2.4 Model-based aerosol forcing sets

Two “synthetic” volcanic aerosol forcing sets were constructed based on a 12-member ensemble of simulations of a Pinatubo-like eruption using the MAECHAM5-HAM coupled aerosol–climate model with  $\text{SO}_2$  injections of 17 Tg and prescribed climatological sea surface temperatures (Tooney et al., 2011). Figure 3 shows lower stratospheric zonal mean temperature anomalies (at 100 hPa) and zonal wind anomalies (at 50 hPa) for these simulations, in comparison with ERA-Interim post-volcanic anomalies described in Sect. 2.1. Most of the MAECHAM5-HAM ensemble members (roughly 9/12) show characteristics of a strengthened polar vortex in the lower stratosphere, as quantified as negative temperature anomalies at polar latitudes and positive zonal wind anomalies between 60 and 80° N in Fig. 3. However, the ensemble variability of the simulations is pronounced, with three members showing a weakened polar vortex with positive temperature anomalies over the polar cap and negative wind anomalies between 60 and 80° N. From the full 12-member ensemble, two subsets were defined based on the zonal wind anomalies, with strong and weak vortex composites (hereafter SVC and WVC) defined respectively as the average of the three realizations with the most positive and most negative zonal wind anomalies at 50 hPa and 70° N. Aerosol properties (aerosol extinction at 0.55  $\mu\text{m}$  and effective radius) for these two composites were collected for use in MPI-ESM simulations. SVC and WVC zonal mean AOD time series, scaled to 1  $\mu\text{m}$  to be consistent

with the observation-based AOD time series, are shown in Fig. 2.

## 2.5 Experiments

The forcing sets described above were used to force four 16-member ensemble simulations of the Pinatubo eruption time period. The number of MPI-ESM realizations used here is therefore notably greater than the three MPI-ESM realizations used in prior single- (Schmidt et al., 2013) or multi-model (Charlton-Perez et al., 2013; Driscoll et al., 2012) investigations of the CMIP5 historical simulations. Ten of the 16 unique initial condition states (at June 1991) were taken from 10 independent, pre-existing CMIP5 historical simulations. In order to increase the ensemble size, six of the historical simulations were restarted in 1980 with a small atmospheric perturbation applied, and integrated until 1991. All simulations were therefore forced with S98 volcanic forcing up until June 1991, at which point forcing either continued as S98 or switched to one of the other forcings.

A control ensemble (CTL) is based on the 5 year period 1986–1990 for the original 10 historical simulations used to produce the initial conditions, comprising in total 50 years, during which the other external forcings are negligibly different from 1991–1992 conditions. Anomalies for the volcanic ensembles are computed by differencing ensemble mean results with the CTL ensemble mean.

Observations imply that the NH winter vortex response to volcanic forcing may last for 2 years. While considering the results for the first two winters together certainly increases the ensemble size, it is quite possible that the mechanisms leading to vortex response are different in the first and second winters after an eruption. The magnitude of aerosol forcing will be different for the two winters for any forcing set,

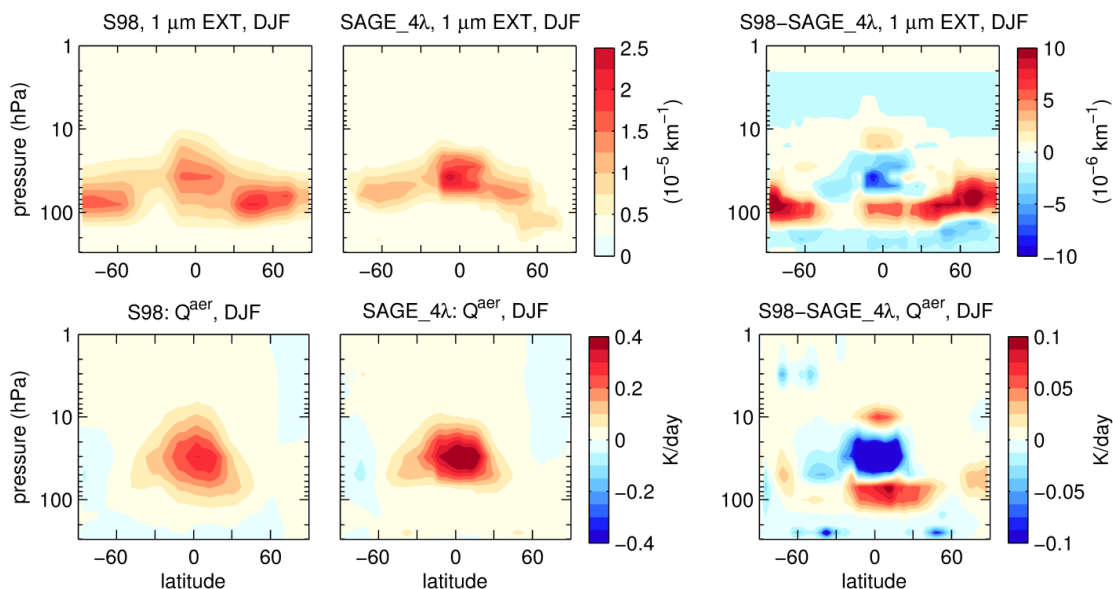


**Figure 4.** (top) Latitude–pressure distributions of 1  $\mu\text{m}$  aerosol extinction in the S98 and SAGE\_4 $\lambda$  volcanic aerosol forcing sets in first DJF after Pinatubo (winter 1991/92). (bottom) Aerosol radiative heating ( $Q^{\text{aer}}$ ) as computed within the MPI-ESM model for each forcing set. Right-hand column shows S98-SAGE\_4 $\lambda$  differences for both 1  $\mu\text{m}$  extinction and  $Q^{\text{aer}}$ .

with typically stronger aerosol forcing occurring in the first winter. Such temporal changes are likely larger than differences between the different forcing sets used in this study. With these potential complications in mind, in order to simplify the analysis and interpretation of the model results in this study, we choose to focus our analysis only on the first winter after the Pinatubo eruption.

Unless otherwise stated, results shown are ensemble means. Confidence intervals (95 % level) are calculated for differences between forced and CTL ensemble means and the differences between the forced ensemble means using a bootstrapping technique, with 1000 resamples of the original ensembles. For example, for each latitude and pressure level, and for each forced ensemble, 1000 bootstrapped sample means are produced by sampling the 16 ensemble member values with replacement, resulting in an approximation of the uncertainty distribution for the mean value. The same process is applied to the CTL ensemble, with  $n = 50$ . The difference between the two bootstrapped distributions defines the uncertainty in the mean difference, and is used to define the 95 % confidence interval of the ensemble mean difference. A parallel procedure is used to define the confidence intervals for the differences of two volcanically forced ensembles.

### 3 Results

#### 3.1 Radiative forcing

Latitude–pressure plots of zonal mean DJF 1  $\mu\text{m}$  extinction (EXT) are shown in Fig. 4 for the S98 and SAGE\_4 $\lambda$  forcing sets. A major difference between the two forcing sets is the vertical distribution of extinction in the tropics, with SAGE\_4 $\lambda$  extinction being more constrained to the lower stratosphere, compared to S98 which has considerable extinction extending down into the upper troposphere. This difference in tropical extinction is the result of improvements in the SAGE\_4 $\lambda$  retrieval: the S98 vertical distribution in the tropics is very likely unrealistic (Arfeuille et al., 2013). The two forcing sets also differ in terms of the magnitude of tropical extinction, with SAGE\_4 $\lambda$  having stronger extinction in the tropical lower stratosphere for all wavelengths greater than 0.55  $\mu\text{m}$ . Differences in extinction magnitude are also apparent in the high-latitude lower stratosphere of both hemispheres, with SAGE\_4 $\lambda$  extinction much smaller than that of S98.

Direct aerosol radiative heating rates ( $Q^{\text{aer}}$ ) are computed by performing radiative transfer calculations at each model time step twice, once with and once without the volcanic aerosols (as in Stenchikov et al., 1998). We have calculated  $Q^{\text{aer}}$  for single realizations of each forced ensemble.

Net (long wave + short wave)  $Q^{\text{aer}}$  for DJF for the two observation-based forcing sets is shown in Fig. 4.  $Q^{\text{aer}}$  values are positive over most of the stratosphere for both S98 and SAGE\_4 $\lambda$  forcings, with highest magnitude in the tropical lower stratosphere at approximately 30 hPa, just north of

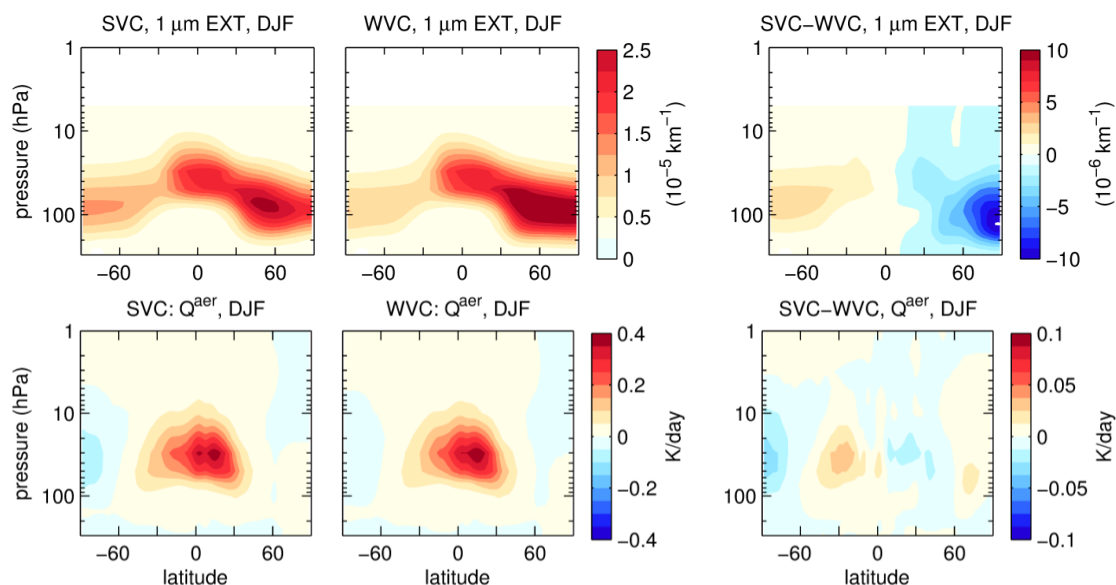


**Figure 5.** (top) Latitude–pressure distributions of 1  $\mu\text{m}$  aerosol extinction in the SVC and WVC volcanic aerosol forcing sets in first DJF after Pinatubo (winter 1991/92). (bottom) Aerosol radiative heating ( $Q^{\text{aer}}$ ) as computed within the MPI-ESM model for each forcing set. Right-hand column shows SVC–WVC differences for both 1  $\mu\text{m}$  extinction and  $Q^{\text{aer}}$ .

the equator. Like the extinction values (Fig. 4, upper row), S98 heating rates are spread over a larger vertical extent than SAGE\_4 $\lambda$  heating rates: at the equator, S98 heating rates  $>0.1 \text{ K day}^{-1}$  extend from  $\sim 100 \text{ hPa}$  upwards whereas for the SAGE\_4 $\lambda$  forcing set, heating rates  $>0.1 \text{ K day}^{-1}$  begin  $\sim 60 \text{ hPa}$ . Like the extinction at 1  $\mu\text{m}$  (and longer wavelengths) SAGE\_4 $\lambda$  forcing leads to stronger  $Q^{\text{aer}}$ , with maximum values of  $0.5 \text{ K day}^{-1}$  compared to max values of  $0.3 \text{ K day}^{-1}$  for S98. Although minor compared to the differences in the tropical stratosphere, there are differences in  $Q^{\text{aer}}$  in the NH polar latitudes, with S98 leading to slightly larger  $Q^{\text{aer}}$  values in the NH polar lower stratosphere than for SAGE\_4 $\lambda$ .

Figure 5 shows DJF 1  $\mu\text{m}$  aerosol extinction for the SVC and WVC forcing sets. Compared to the observation-based forcing sets, both model-based forcing sets have greater magnitudes of aerosol extinction, especially in the high latitudes. Such differences likely arise from a combination of (1) underestimates in the observation-based forcing sets due to saturation effects, especially in the weeks directly following the eruption, and (2) potential errors in the model simulations, in terms of either general model deficiencies or errors in the model formulation in regard to the actual Pinatubo eruption (e.g.  $\text{SO}_2$  injection amount or height). The model-based extinctions also have stronger gradients (both vertical and horizontal) across the tropopause compared to the observation-based forcing sets. These differences, especially in the vertical, are likely due to the limited vertical resolution of the observations. The primary difference between the SVC and WVC forcings is the hemispheric partitioning of the aerosol extinction, with WVC having larger extinctions in the NH

than SVC. We interpret this difference as a result of wave driven circulation in the NH: in cases of strong NH wave forcing in the original MAECHAM5–HAM runs, a stronger residual circulation transports more aerosol from the tropical region towards the NH, while also disturbing the NH polar vortex. Therefore, by selecting cases of weak polar vortex, we also select cases of strong northward aerosol transport. Another major difference is the magnitude of extinction in the NH high latitudes, and therefore the gradient in extinction around  $60^\circ\text{N}$ . The stronger aerosol extinction gradient in the SVC forcing set is obviously a result of the strong vortex in the MAECHAM5–HAM simulations, which inhibits mixing of aerosol into the polar cap. In the tropics, SVC and WVC have very small differences, and their vertical distribution is almost identical.

$Q^{\text{aer}}$  values from the model-based forcing sets, also shown in Fig. 5, are more similar to the observation-based  $Q^{\text{aer}}$  values than the extinctions: the differences in high-latitude extinction have relatively little impact on the  $Q^{\text{aer}}$  differences due to the much weaker long wave radiation field here than in the tropics. Differences in  $Q^{\text{aer}}$  between the two model-based forcing ensembles are relatively small (compared to differences between the two observation-based forcing ensembles), and are characterized primarily by the north–south shift between the two forcing sets, and the gradients in  $Q^{\text{aer}}$  at  $60^\circ\text{S}$  and  $60^\circ\text{N}$ . At high latitudes,  $Q^{\text{aer}}$  values are apparently not strongly dependent on the aerosol extinction; for example, SVC has smaller aerosol extinction values in polar latitudes than WVC, but shows larger  $Q^{\text{aer}}$ . This is likely due to the fact that the net (absorption–emission) long wave heating rate is strongly temperature dependent because of the

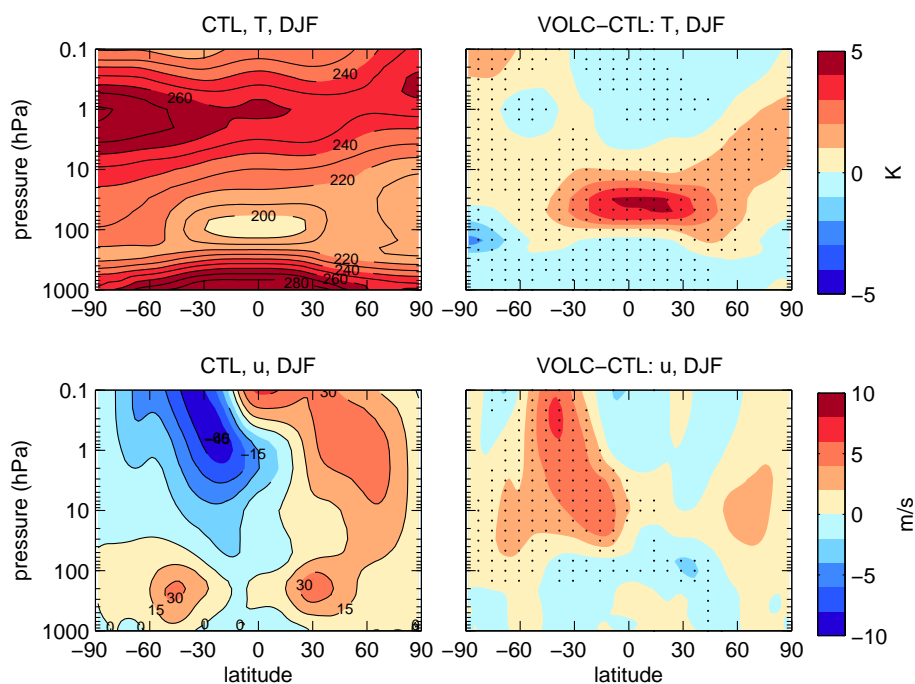


**Figure 6.** DJF temperature (top) and zonal wind (bottom) from the CTL ensemble (left) and anomalies for the VOLC grand ensemble (right). Stippling highlights anomalies that are significant at the 95 % confidence level based on a bootstrapping algorithm.

temperature dependence of the emission. As shown below, the SVC ensemble is characterized by a colder polar vortex than for WVC, which should lead to less emission and thus larger net heating.

### 3.2 Temperature and zonal wind response

In order to determine which thermal and dynamical responses to the volcanic forcings are robust across the different forcings, results are first examined by concatenating the 64 volcanic simulations into one “grand” ensemble (VOLC), with ensemble mean anomalies of temperature and zonal wind shown in Fig. 6.

Significant and robust temperature responses in the volcanic simulations include positive anomalies in the tropical lower stratosphere and negative temperature anomalies in the troposphere, extending to the surface between approximately  $70^{\circ}$  S– $45^{\circ}$  N. In the NH high-latitude stratosphere, the temperature anomaly structure for the VOLC ensemble is roughly consistent with that shown by Schmidt et al. (2013) for three MPI-ESM realizations (using S98 forcing), with positive temperature anomalies in the upper stratosphere and mesosphere. However, while temperature anomalies for the VOLC ensemble are significant throughout most of the tropopause and lower-to-middle stratosphere, anomalies in the NH polar region are generally not significant.

Significant zonal wind responses in the VOLC ensemble include weakening of the subtropical jets at  $\sim 30^{\circ}$  and  $\sim 100$  hPa of both hemispheres by  $2\text{--}4\text{ m s}^{-1}$ , and a weaken-

ing of the SH stratospheric easterlies by  $4\text{--}6\text{ m s}^{-1}$ . Grand ensemble mean zonal wind anomalies in the NH high-latitude stratosphere reach a maximum of  $\sim 2\text{--}4\text{ m s}^{-1}$ , and are not significant.

Temperature and zonal wind anomalies are shown separately for the observation- and model-based forcing ensembles in Figs. 7 and 8, respectively. For the observation based forcings S98 and SAGE\_4 $\lambda$  (Fig. 7), the general features are consistent with the VOLC grand ensemble. In agreement with  $Q^{\text{aer}}$  of Fig. 4, SAGE\_4 $\lambda$  tropical temperature anomalies are greater in magnitude, with peak values of 4.8 K compared to 3.6 K for S98. Temperature anomalies are also shifted in height between the two ensembles, with peak temperature anomalies located at 30 hPa for SAGE\_4 $\lambda$ , compared to 50 hPa for S98. Differences in tropical temperature anomalies between the two ensembles (right-most column of Fig. 7) are significant at the 95 % confidence level between approximately 200 and 20 hPa. The SAGE\_4 $\lambda$  ensemble shows slightly larger warming in the polar upper stratosphere, although the difference between S98 and SAGE\_4 $\lambda$  is not significant.

In the NH high latitudes, the S98 ensemble shows a weak ( $2\text{--}3\text{ m s}^{-1}$ ) increase in westerly wind, while the SAGE\_4 $\lambda$  ensemble shows a weak ( $3\text{--}4\text{ m s}^{-1}$ ) negative wind anomaly in the upper stratosphere/mesosphere. Differences between the two ensembles are not significant in the midlatitudes to high latitudes.

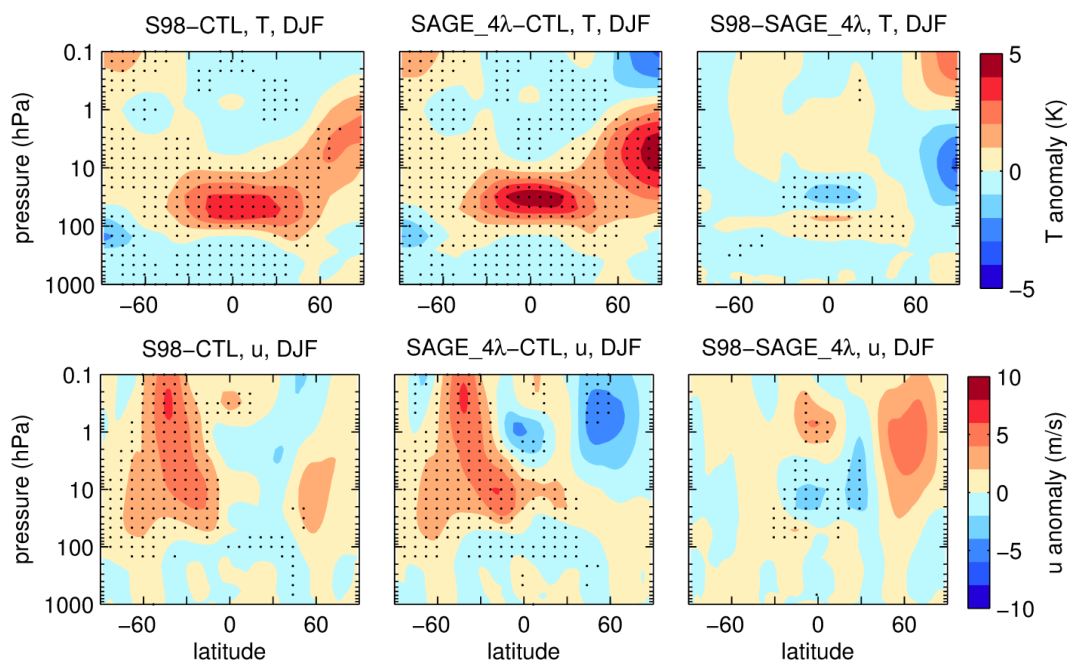


**Figure 7.** Temperature and zonal wind response of the observation-based volcanic forced ensembles. Shown are DJF anomalies for the (left) S98 and (middle) SAGE\_4 $\lambda$  ensembles, and (right) the difference between the two ensembles for (top) temperature and (bottom) zonal wind. Stippling highlights anomalies that are significant at the 95 % confidence level based on a bootstrapping algorithm.

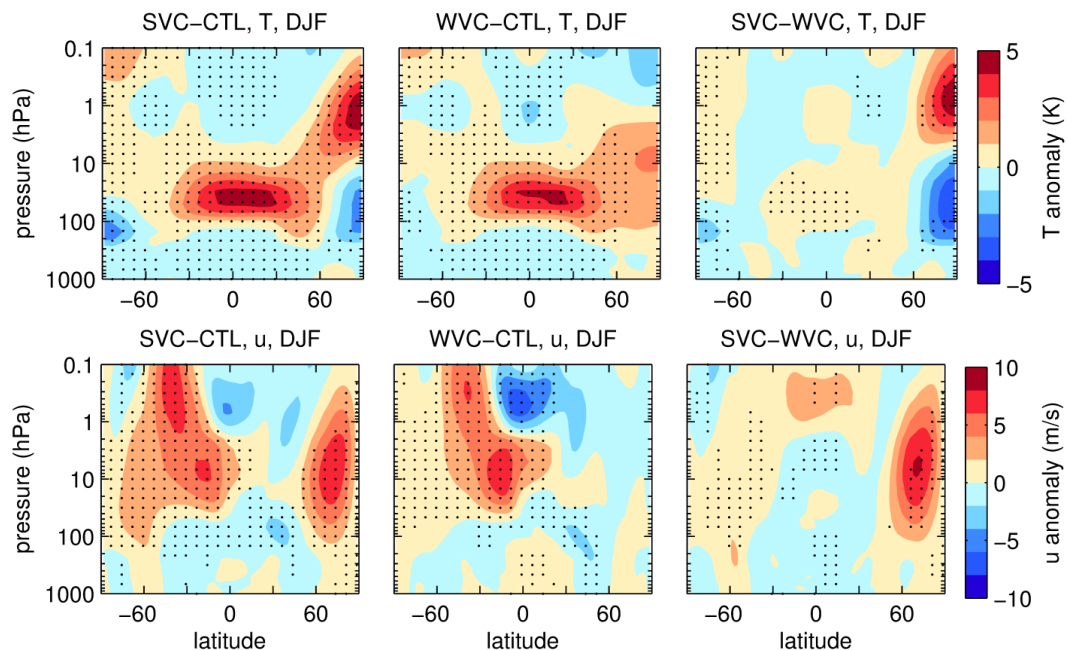


**Figure 8.** Temperature and zonal wind response of the model-based volcanic forced ensembles. Shown are DJF anomalies for the (left) SVC and (middle) WVC ensembles, and (right) the difference between the two ensembles for (top) temperature and (bottom) zonal wind. Stippling highlights anomalies that are significant at the 95 % confidence level based on a bootstrapping algorithm.

For the model-based forcing ensembles SVC and WVC (Fig. 8), temperature anomalies in the tropics and midlatitudes are quite similar in structure between the two ensem-

bles and similar to the grand ensemble mean. In the NH high latitudes, however, the temperature responses are quite different in structure between the two ensembles. The SVC ensem-

ble produces an NH high-latitude temperature anomaly pattern with significant warming in the upper stratosphere and lower mesosphere. WVC, on the other hand, gives a temperature anomaly pattern with insignificant positive temperature anomalies in the polar lower and middle stratosphere. Differences between the two forcing sets are significant in the polar lower and upper stratosphere.

Zonal wind anomalies for the model-based forcing ensembles follow from the temperature anomalies. The SVC ensemble produces a significant strengthening of the NH polar vortex, with peak zonal wind anomalies  $6\text{--}8\text{ m s}^{-1}$ . The WVC ensemble produces no significant change in NH vortex winds. The difference between the vortex response in the SVC and WVC ensembles is significant in the polar lower stratosphere, and in the mid-to-upper stratosphere at the highest latitudes ( $70\text{--}90^\circ\text{ N}$ ).

DJF zonal mean zonal wind at  $60^\circ\text{ N}$  and 10 hPa for each realization of each ensemble is shown in Fig. 9. Ensemble means with 95 % confidence intervals are also shown. The mean of the control ensemble is marked by a horizontal dashed line. Consistent with results discussed above, only the SVC ensemble shows a significant zonal wind response to volcanic forcing, with an ensemble mean 95 % interval that excludes the control mean. In terms of individual ensemble members, 13/16 members of the SVC ensemble have zonal mean wind greater than the control mean, although all of the members lie within the natural variability of the control ensemble. Three SVC members have zonal winds weaker than the control; as such, the response to SVC forcing is not totally robust and the increase in ensemble mean vortex strength appears to represent a change in the probability of weak vs. strong vortex states. The WVC and S98 ensembles show ensemble means and spreads very similar to the control ensemble, with S98 showing a weak and insignificant positive anomaly in wind strength. The SAGE<sub>4λ</sub> ensemble shows an ensemble mean equal to that of the control ensemble, but interestingly shows some evidence of a decrease in ensemble variability.

### 3.3 Wave-driven circulation response

For all ensembles, we have computed transformed Eulerian mean (TEM) diagnostics (Andrews et al., 1987), including Eliassen–Palm (EP) fluxes, the meridional residual mass circulation stream function ( $\psi^*$ ), the residual vertical velocity ( $\bar{w}^*$ ), and temperature tendencies due to vertical residual advection. Ensemble means of these quantities have been compared to values from the control ensemble in order to compute post-volcanic anomalies in the first NH winter. As for the temperature and zonal wind anomalies, selected TEM quantities are examined first in terms of the grand VOLC ensemble in Fig. 10.

It is well known that the variability of polar vortex strength is largely controlled by planetary wave drag, and therefore depends on the upward wave flux from the troposphere into

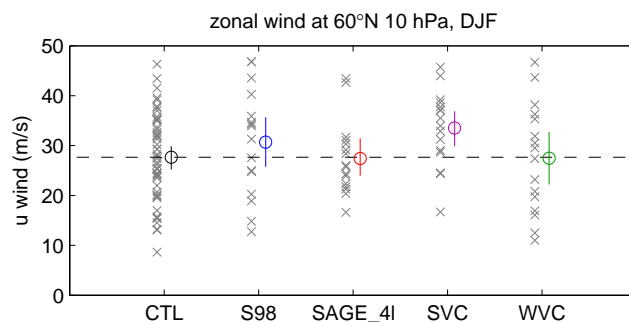


**Figure 9.** DJF zonal wind at  $60^\circ\text{ N}$  and 10 hPa for the CTL ensemble and the volcanically forced ensembles S98, SAGE<sub>4λ</sub>, SVC and WVC. Individual ensemble members shown as grey symbols. Ensemble means shown in coloured symbols, with vertical whiskers representing the 95 % confidence interval of the ensemble mean. Dashed horizontal line shows the ensemble mean of the CTL ensemble.

the stratosphere (Newman et al., 2001; Polvani and Waugh, 2004). The vertical component of EP-flux ( $F_z$ ) is a commonly used proxy for the amount of wave activity entering and propagating through the stratosphere. Figure 10 shows DJF  $F_z$  for the control ensemble and anomalies for the VOLC grand ensemble. Around the tropopause ( $\sim 100\text{--}200\text{ hPa}$ ),  $F_z$  anomalies in the VOLC ensemble are negative in the mid-latitude ( $30\text{--}45^\circ$ ) regions of both hemispheres, and generally positive in the midlatitudes to high latitudes ( $45\text{--}90^\circ\text{ N}$ ). Positive  $F_z$  anomalies are significant throughout the SH stratosphere, while in the NH, significant positive  $F_z$  anomalies occur around  $60^\circ\text{ N}$  and 100 hPa, and extend upwards, slanting equatorward with height.

Convergence of EP-flux (or negative values of EP-flux divergence, EPFD) leads to wave drag, a slowing of the wintertime westerly (eastward) zonal wind and a poleward residual circulation. Enhanced wave drag in volcanic simulations is found throughout the SH stratosphere and in the midlatitude NH middle stratosphere (around  $30^\circ\text{ N}$ , 10 hPa, Fig. 10d). Wave drag in the latter location is especially important for forcing the residual circulation (Shepherd and McLandress, 2011). Figure 10e and f show the CTL and VOLC anomalies of the meridional residual circulation stream function. The poleward NH residual circulation stream function is found to be enhanced in the VOLC ensemble.

The volcanically induced residual circulation anomalies drive adiabatic heating anomalies where vertical motions are induced. Temperature tendency anomalies due to residual vertical velocity (hereafter  $dT_{\bar{w}^*}$ , Fig. 10g, h) show clearly the tropical cooling associated with anomalous vertical upwelling, and heating at the midlatitudes and high latitudes due to anomalous downwelling.

The terms  $dT_{\bar{w}^*}$  and  $Q^{\text{aer}}$  are found to dominate the temperature tendency budget compared to other terms in the TEM diagnostics. Therefore, the temperature anomalies found in the volcanic simulations can be understood to be pri-

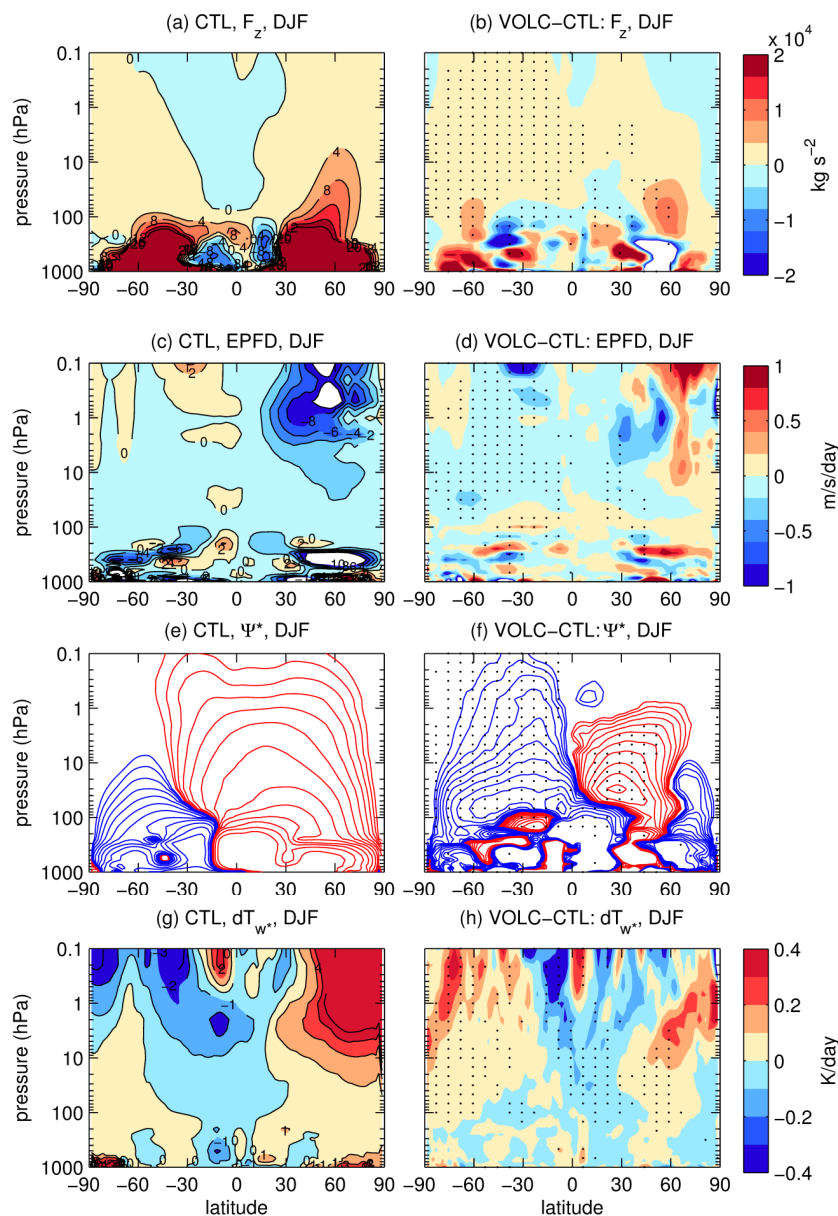


**Figure 10.** Selected TEM diagnostics for (left) the CTL ensemble and (right) anomalies for the VOLC grand ensemble. Shown are (a, b) vertical component of EP-flux, (c, d) EP-flux divergence, (e, f) residual circulation streamfunction and (g, h) heating due to residual vertical advection. Contours in (a) are in units of  $1 \times 10^4 \text{ kg s}^{-2}$ . Stream function contours in (e) and (f) are red for positive values and blue for negative values, and are log-spaced, ranging from 10 to  $1 \times 10^4 \text{ kg m}^{-1} \text{ s}^{-1}$  in panel (e) and 1 to  $100 \text{ kg m}^{-1} \text{ s}^{-1}$  in panel (f).

marily the result of the direct (diabatic) aerosol heating  $Q^{\text{aer}}$ , and the indirect, dynamical (adiabatic) heating  $dT_{\overline{w}^*}$ . These terms, along with the corresponding temperature anomalies, are shown for each of the volcanic ensembles as lower stratosphere (100–20 hPa) averages in Fig. 11.

Ensemble mean temperature anomalies show roughly similar behaviour in the tropics and midlatitudes (0–55° N) for all ensembles. In the NH polar latitudes, weak positive temperature anomalies are simulated for the S98, SAGE\_4λ and WVC ensembles, and negative anomalies for the SVC en-

semble.  $Q^{\text{aer}}$  peaks in the tropics and decays to zero between 30 and 60° N.  $dT_{\overline{w}^*}$  is negative in the tropics, opposing the  $Q^{\text{aer}}$  heating, and becomes generally positive in the extratropics where downward advection occurs. In the high latitudes,  $dT_{\overline{w}^*}$  is positive for S98, SAGE\_4λ and WVC, but negative for SVC, consistent with the temperature anomalies (Fig. 8). It is thus clear that the differences in temperature anomalies at high latitudes, and therefore the temperature gradients around 60° N, result from differences in  $dT_{\overline{w}^*}$  between the ensembles. The effect of differences in temperature

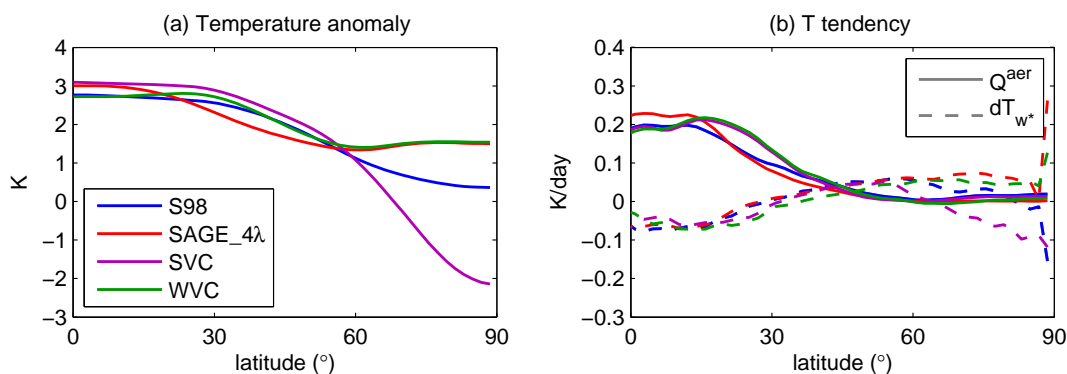


**Figure 11.** Lower stratospheric (100–20 hPa), DJF average thermodynamic quantities from the four volcanically forced ensembles: (a) temperature anomalies, (b) temperature tendencies due to aerosol radiative heating  $Q^{\text{aer}}$  (solid lines) and vertical advection ( $dT_{\overline{w}^*}$ , dashed lines).

tendencies on temperature anomalies is likely amplified at higher latitudes since radiative damping timescales increase with latitude in the lower stratosphere (Newman and Rosenfield, 1997). These results underscore the point that temperature gradients at the high latitudes are controlled by the structure of the volcanically induced residual circulation anomalies rather than the direct aerosol heating.

Differences in the dynamical responses to the SVC and WVC volcanic forcings are further explored by examining TEM diagnostics for these ensembles. As in the VOLC grand ensemble, both model-based forced ensembles show positive  $F_z$  anomalies throughout the SH stratosphere and negative anomalies in the subtropical tropopause region (Fig. 12a, b). Positive  $F_z$  anomalies are found at the NH high-latitude lower stratosphere, extending upwards and slanting equatorward with height. However, these positive  $F_z$  anomalies are much stronger (and significant only) in the WVC ensemble.

As in the VOLC ensemble, negative EP-flux divergence (wave drag) is significantly enhanced in the SH stratosphere and in the NH midlatitude middle stratosphere in both the SVC and WVC ensembles (Fig. 10d, e). NH wave EP-flux divergence anomalies are notably stronger in the WVC ensemble between 10 and 100 hPa and 30–60° N; differences between the two ensembles are significant around 100 hPa and 60° N. Residual circulation anomalies (Fig. 12g, h) show significant poleward circulation cells in both hemispheres. Notable differences in the form of the induced residual circulation cells between the two ensembles exist in the lower and middle NH stratosphere, with circulation cells confined to 0–45° N in the SVC ensemble, and extending 0–90° N in the WVC ensemble. These differences are significant in around 100 hPa and 60° N, and as such appear related to the differences in EP-flux divergence discussed above. Temperature tendency anomalies due to residual vertical velocity ( $dT_{\overline{w}^*}$ , Fig. 10j, k) show that the broad residual circulation anomaly cell in the WVC ensemble leads to dynamical heating of the lower stratosphere extending from ~45–90° N, while the narrower poleward cell in SVC leads to significant heating

only in the midlatitude (45–60° N) lower stratosphere. Differences in dynamical warming are marginally significant in the polar lower stratosphere, consistent with the differences in EP-flux divergence and residual circulation.

The TEM fields of Fig. 12 thus show that the significant difference in polar vortex zonal wind response to the SVC and WVC volcanic forcings comes about due to differences in the wave activity propagating upwards into the stratosphere from the troposphere. This mechanism is further explored in Fig. 13 for all volcanic ensembles. Figure 13 (left) shows the relationship between polar vortex wind ( $u$  at 10 hPa, 60° N, hereafter  $u_{\text{vortex}}$ ) and lower stratosphere polar temperature ( $T$  at 50 hPa, 60–90° N average, hereafter  $T_{\text{vortex}}$ ). Individual ensemble members are shown by circular markers, while ensemble mean values are shown as triangles on the bottom and right-hand axes. The compact linear relationship between  $u_{\text{vortex}}$  and  $T_{\text{vortex}}$  apparent in the control run is shifted in the volcanic simulations: for a given  $T_{\text{vortex}}$ , the associated  $u_{\text{vortex}}$  is typically  $\sim 5 \text{ m s}^{-1}$  stronger in the volcanic runs than in CTL. The SVC ensemble mean  $T_{\text{vortex}}$  is similar to the CTL ensemble mean, and correspondingly, the SVC  $u_{\text{vortex}}$  is larger than the CTL ensemble mean by 5–10  $\text{m s}^{-1}$ . In contrast, the other volcanic ensembles all show increases in  $T_{\text{vortex}}$ , and correspondingly,  $u_{\text{vortex}}$  for these ensembles is less than that of SVC, and similar to the CTL ensemble mean value.

Polar lower stratosphere temperatures are related to upward EP-flux in the midlatitudes (Newman et al., 2001; Polvani and Waugh, 2004). In Fig. 13b,  $u_{\text{vortex}}$  is plotted vs.  $F_z$  at 100 hPa averaged over 45–75° N (hereafter  $F_{z,100}$ , a common scalar metric for wave activity entering the extratropical stratosphere). Polar vortex strength,  $u_{\text{vortex}}$ , is seen to be stronger for any particular  $F_{z,100}$  value in the volcanic runs compared to the CTL ensemble. For the SVC ensemble,  $F_{z,100}$  is comparable to the CTL value, and the  $u_{\text{vortex}}$  anomaly is 5–10  $\text{m s}^{-1}$ . The other ensembles show positive anomalies in  $F_{z,100}$ ; the zonal wind of these volcanic ensembles are thus reduced due to the increased wave activity

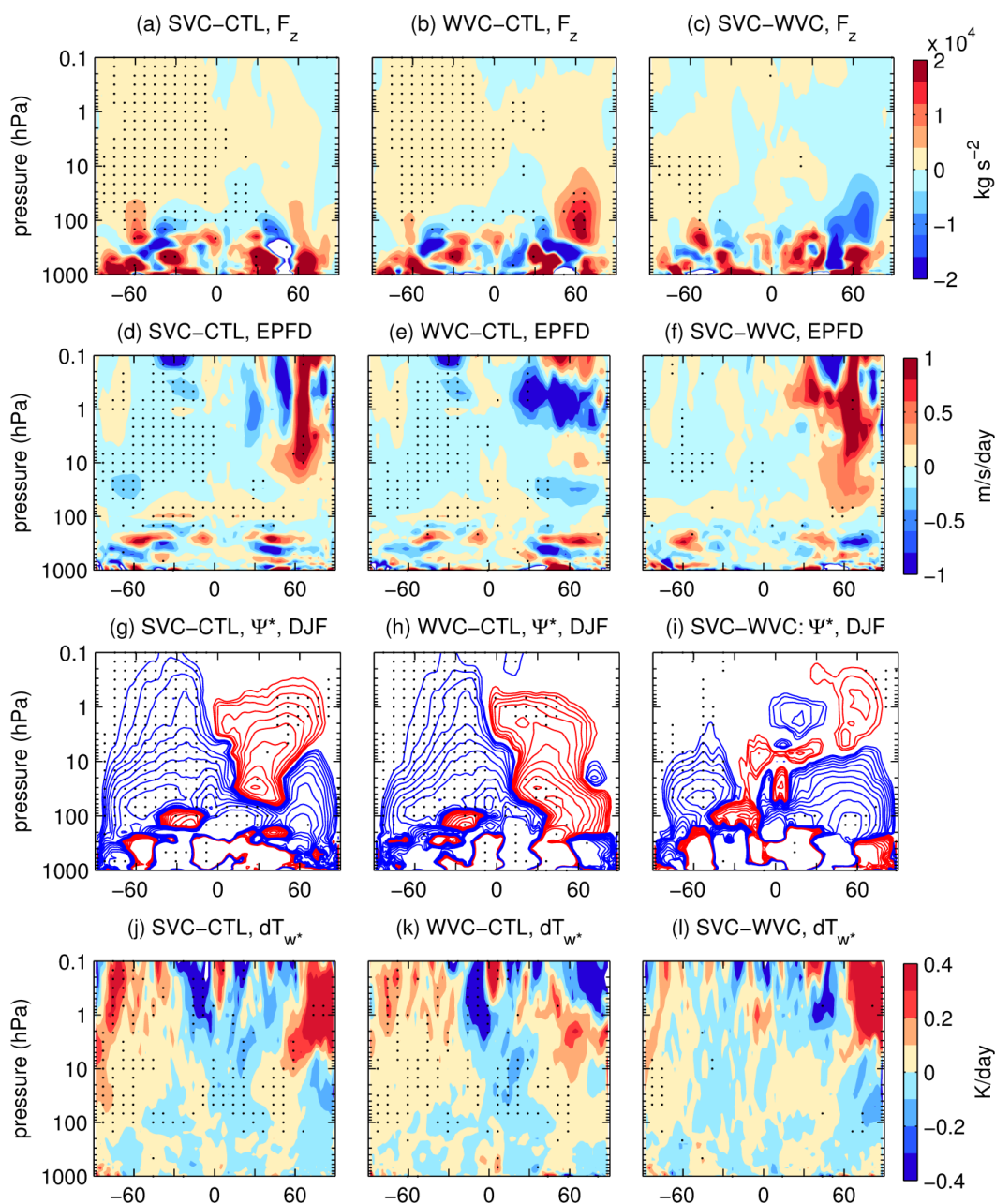


**Figure 12.** Selected TEM diagnostics for the SVC and WVC forced ensembles. Shown are DJF anomalies for the (left) SVC and (middle) WVC ensembles, and (right) the difference between the two ensembles for (a, b, c) vertical component of EP-flux, (d, e, f) EP-flux divergence, (g, h, i) residual circulation streamfunction and (j, k, l) heating due to residual vertical advection. Stream function contours in panels (g, h, i) are red for positive values and blue for negative values, and are log-spaced ranging from 1 to  $100 \text{ kg m}^{-1} \text{ s}^{-1}$ .

and hence wave drag. Post-volcanic anomalies in  $F_{z,100}$  thus exert a negative feedback on the wind anomalies driven by changes in the lower stratosphere temperature gradient.

#### 4 Discussion

A major result of the preceding sections is that the temperature structure of the lower stratosphere in post-volcanic

winters in the high latitudes is controlled primarily by induced residual circulation anomalies. Post volcanic-eruption enhancement of the stratospheric residual circulation (or Brewer-Dobson circulation) has been suggested based on previous model studies (Pitari and Mancini, 2002; Pitari, 1993). Graf et al. (2007) assessed the observational record and found evidence of increased winter stratospheric wave activity after three eruptions (Agung, El Chichón and

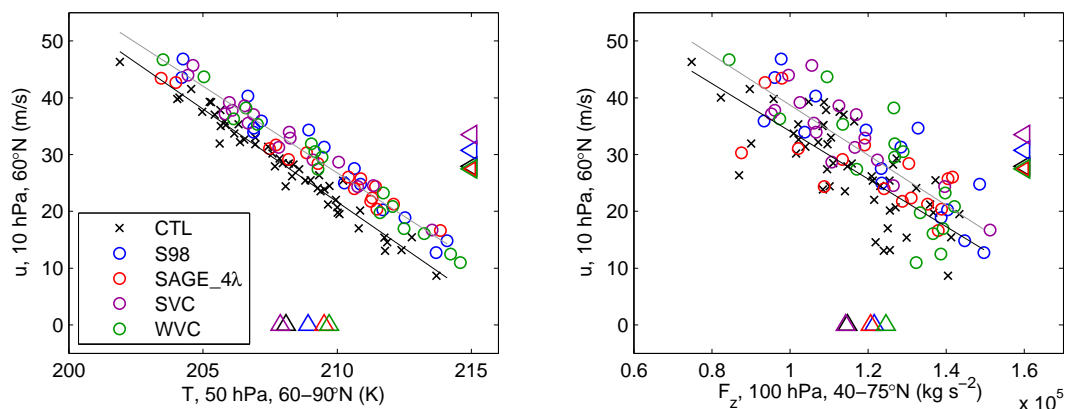


**Figure 13.** Scatter plots of vortex wind, temperature and wave forcing for the CTL and four volcanically forced ensembles. All quantities are averaged over the NH winter (DJF). Shown are (left) zonal wind at 10 hPa, 60° N plotted against temperature at 50 hPa, 60–90° N averaged, and (right) zonal wind at 10 hPa, 60° N plotted against the vertical component of EP-flux averaged over 40–75° N. Individual forced ensemble members are shown by coloured circles, and the CTL ensemble members by black crosses. Ensemble mean values of the quantities plotted on the horizontal and vertical axes of each panel are shown by coloured (black) triangles for the forced (CTL) ensembles along the bottom and right-hand axes.

Pinatubo). Poberaj et al. (2011) showed that anomalously strong EP-fluxes occurred in the SH after Pinatubo. Such increases in winter stratospheric wave activity may be a result of changes in the wave propagation conditions of the stratosphere following aerosol radiative heating, allowing more planetary waves to propagate upwards. Similar arguments explain climate models' predicted increase in future stratospheric residual circulation due to changes in the atmospheric temperature structure due to climate change (Garcia and Randel, 2008; McLandress and Shepherd, 2009; Shepherd and McLandress, 2011), which also enhances the meridional temperature gradient in the lower stratosphere, albeit at lower altitudes.

The residual circulation anomalies induced by the volcanic forcing in the ensembles strengthen the climatological residual circulation, although the structure of the anomalies is different to the climatology. For example, the induced upwelling is centred on the equator whereas the maximum climatological upwelling is centred in the summer hemisphere, and the induced upwelling is strongest above the level of maximum aerosol radiative heating, and even negative below. This latter point may explain why post-Pinatubo anomalies in tropical upwelling are not apparent in observational records, which are usually displayed as time series of upwelling in the lower stratosphere (Seviour et al., 2012). We have shown that increased wave activity and wave drag in both hemispheres is a robust response to volcanic aerosol forcing in the MPI-ESM, and therefore a component of the residual circulation anomalies in the volcanically forced simulations results from wave drag anomalies. However, given the fact that maximum anomalous tropical upwelling occurs at and above the location of maximum aerosol radiative heating in the tropics, it seems possible that there is also a diabatic component

to the anomalous residual circulation, forced directly by the aerosol radiative heating, as suggested by previous studies (e.g. Aquila et al., 2013; Pitari and Mancini, 2002).

The lack of a robust NH polar vortex response to the Pinatubo forcings used here does not necessarily rule out the possibility that other forcings could produce significant vortex responses. Most obviously, the magnitude of the volcanic forcing may be essentially important. Toohey et al. (2011) found a significant vortex response to a near-super eruption volcanic forcing, which likely produced a much stronger direct aerosol radiative heating gradient in the midlatitudes to high latitudes. Similarly, Bittner et al. (“Sensitivity of the Northern Hemisphere winter stratosphere variability to the strength of volcanic eruptions”, submitted manuscript) find a significant response of the MPI-ESM NH polar vortex to volcanic forcing representing that of the 1815 eruption of Tambora. It is also important that our simulations do not include possible chemical depletion of stratospheric ozone brought about by the presence of volcanic aerosols, or ozone anomalies due to changes in the residual circulation. Induced changes in the meridional structure of stratospheric ozone can also affect temperature gradients in the lower stratosphere (Muthers et al., 2014), and may be a significant feedback in the response of the polar vortex to volcanic forcing.

While the SAGE\_4λ volcanic forcing set is almost certainly a more accurate reconstruction of the true aerosol evolution than S98 in many aspects, e.g. the vertical distribution of aerosol extinction in the tropics, it does not produce the expected increase in NH polar vortex strength in simulations with the MPI-ESM. It actually leads to a somewhat weaker vortex than the S98 forcing, which is especially surprising given that it produces stronger radiative heating in the tropical lower stratosphere than S98.

The model-based SVC forcing was the only forcing to produce a significant vortex strengthening. Differences in simulated vortex response between the different ensembles imply sensitivity in vortex response to the exact structure of the volcanic forcing. These differences between the ensembles, and especially the significant response of SVC ensemble, should perhaps be taken with a grain of salt: the large variability of wave drag and vortex dynamics necessitates the use of large ensembles in order to negate the impact of variability on the ensemble means. While our ensemble size of 16 is larger than most prior single-model volcanic studies, it may still be insufficient to unambiguously identify significant high-latitude responses from volcanic forcing. Furthermore, given the anomalous heating of the lower stratosphere in volcanic simulations, it could be the case that insignificant anomalies in residual circulation lead to significant anomalies in ensemble mean temperature gradients and therefore zonal wind. Nevertheless, planetary wave propagation through the tropopause region has been shown to be quite sensitive to local vertical and meridional gradients in zonal wind and temperature (e.g. Chen and Robinson, 1992). It is plausible that small differences in the structure of the prescribed volcanic aerosol forcing, and resulting radiative heating, temperature and wind, could have relatively large impacts on wave propagation.

## 5 Conclusions

In simulations of the post-Pinatubo eruption period with the MPI-ESM with four different volcanic aerosol forcings, an enhanced polar vortex – which is expected based on limited observations and simple theoretical arguments – was not a robust response. The responses that were significant and robust across all four forcings in the NH winter stratospheric include: (1) positive temperature anomalies in the lower tropical stratosphere, (2) enhanced  $F_z$  in the NH midlatitudes (40–60° N) and wave drag in the midlatitude middle stratosphere, (3) enhanced meridional residual circulation, (4) dynamical cooling of the tropical lower stratosphere and heating of the midlatitude lower stratosphere.

The lack of robust polar vortex response to volcanic aerosol forcing in the MPI-ESM simulations of this work is consistent with the multi-model results of the CMIP5 historical experiments (Charlton-Perez et al., 2013; Driscoll et al., 2012). We have shown that the meridional temperature gradient in the extratropical lower stratosphere induced by volcanic aerosol forcing, and therefore the strength of the induced stratospheric winter polar vortex wind anomalies, is controlled primarily by dynamical heating associated with the induced residual circulation rather than the direct aerosol radiative heating. The vortex response in the model is therefore much less robust than would be expected if it were directly due to the aerosol radiative heating, as it is instead sub-

ject to complexity and variability of wave-mean flow interaction in the winter stratosphere.

Our results further imply that the NH polar vortex response is quite sensitive to the specific structure of the volcanic forcing used. Generally, volcanic forcing leads to an overall increase in resolved wave activity entering the midlatitude to high-latitude stratosphere, and the impact of this wave activity tends to weaken the polar vortex, counteracting the impact of low-latitude heating. However, one volcanic forcing set used here, the model-based SVC forcing, did not significantly affect high-latitude wave activity, and thereby produced a strengthened polar vortex, approximately in line with the expected response. We speculate that such sensitivity is due to the role that minor differences in volcanically induced temperature and wind anomalies play in wave–mean flow interactions in the stratosphere. An alternative theory is that differences in volcanic forcing lead to differences in wave generation in the troposphere. In either case, the results imply that – at least for a Pinatubo magnitude eruption – very accurate reconstructions of volcanic aerosol forcing would be required to reproduce any impact of the aerosols on polar vortex strength in climate model simulations.

*Acknowledgements.* The authors would like to thank Chao Li and Holger Pohlmann for providing model restart fields from MPI-ESM simulations. This work was supported by the Federal Ministry for Education and Research in Germany (BMBF) through the research program “MiKlip” (FKZ:01LP130B(MT);/01LP1130A(CT,MB)). Computations were performed at the German Climate Computer Center (DKRZ). We acknowledge the European Centre for Medium-range Weather Forecasts (ECMWF) for our use of ERA-Interim reanalysis data.

Edited by: Q. Errera

## References

- Andrews, D. G., Holton, J. R., and Leovy, C. B.: *Middle Atmosphere Dynamics*, Academic Press, New York, USA, 1987.
- Aquila, V., Oman, L. D., Stolarski, R., Douglass, A. R., and Newman, P. A.: The response of ozone and nitrogen dioxide to the eruption of Mt. Pinatubo at southern and northern midlatitudes, *J. Atmos. Sci.*, 70, 894–900, doi:10.1175/JAS-D-12-0143.1, 2013.
- Arfeuille, F., Luo, B. P., Heckendorn, P., Weisenstein, D., Sheng, J. X., Rozanov, E., Schraner, M., Brönnimann, S., Thomason, L. W., and Peter, T.: Modeling the stratospheric warming following the Mt. Pinatubo eruption: uncertainties in aerosol extinctions, *Atmos. Chem. Phys.*, 13, 11221–11234, doi:10.5194/acp-13-11221-2013, 2013.
- Baldwin, M. P. and Dunkerton, T. J.: Stratospheric harbingers of anomalous weather regimes, *Science*, 294, 581–584, doi:10.1126/science.1063315, 2001.
- Charlton-Perez, A. J., Baldwin, M. P., Birner, T., Black, R. X., Butler, A. H., Calvo, N., Davis, N. A., Gerber, E. P., Gillett, N.,

- Hardiman, S., Kim, J., Krüger, K., Lee, Y.-Y., Manzini, E., McDaniel, B. A., Polvani, L., Reichler, T., Shaw, T. A., Sigmond, M., Son, S.-W., Toohey, M., Wilcox, L., Yoden, S., Christiansen, B., Lott, F., Shindell, D., Yukimoto, S., and Watanabe, S.: On the lack of stratospheric dynamical variability in low-top versions of the CMIP5 models, *J. Geophys. Res.-Atmos.*, 118, 2494–2505, doi:10.1002/jgrd.50125, 2013.
- Chen, P. and Robinson, W. A.: Propagation of planetary waves between the troposphere and stratosphere, *J. Atmos. Sci.*, 49, 2533–2545, doi:10.1175/1520-0469(1992)049<2533:POPWBT>2.0.CO;2, 1992.
- Christiansen, B.: Volcanic eruptions, large-scale modes in the Northern Hemisphere, and the El Niño–Southern Oscillation, *J. Climate*, 21, 910, doi:10.1175/2007JCLI1657.1, 2008.
- Crowley, T., Zielinski, G., Vinther, B. M., Udisti, R., Kretz, K., Cole-Dai, J., and Castellano, E.: Volcanism and the little ice age, *PAGES news*, 16, 22–23, 2008.
- Dee, D. P., Uppala, S. M., Simmons, A. J., Berrisford, P., Poli, P., Kobayashi, S., Andrae, U., Balmaseda, M. A., Balsamo, G., Bauer, P., Bechtold, P., Beljaars, A. C. M., van de Berg, L., Bidlot, J., Bormann, N., Delsol, C., Dragani, R., Fuentes, M., Geer, A. J., Haimberger, L., Healy, S. B., Hersbach, H., Hólm, E. V., Isaksen, I., Kållberg, P., Köhler, M., Matricardi, M., McNally, A. P., Monge-Sanz, B. M., Morcrette, J.-J., Park, B.-K., Peubey, C., de Rosnay, P., Tavolato, C., Thépaut, J.-N., and Vitart, F.: The ERA-Interim reanalysis: configuration and performance of the data assimilation system, *Q. J. Roy. Meteor. Soc.*, 137, 553–597, doi:10.1002/qj.828, 2011.
- Driscoll, S., Bozzo, A., Gray, L. J., Robock, A., and Stenchikov, G.: Coupled Model Intercomparison Project 5 (CMIP5) simulations of climate following volcanic eruptions, *J. Geophys. Res.*, 117, D17105, doi:10.1029/2012JD017607, 2012.
- Eyring, V. and Lamarque, J.-F.: Overview of IGAC/SPARC Chemistry–Climate Model Initiative (CCMI) community simulations in support of upcoming ozone and climate assessments, *SPARC Newsl.*, 40, 48–66, 2013.
- Garcia, R. R. and Randel, W. J.: Acceleration of the Brewer–Dobson circulation due to increases in greenhouse gases, *J. Atmos. Sci.*, 65, 2731–2739, doi:10.1175/2008JAS2712.1, 2008.
- Gerber, E. P., Butler, A., Calvo, N., Charlton-Perez, A., Giorgetta, M., Manzini, E., Perlwitz, J., Polvani, L. M., Sassi, F., Scaife, A. A., Shaw, T. A., Son, S.-W., and Watanabe, S.: Assessing and understanding the impact of stratospheric dynamics and variability on the Earth system, *B. Am. Meteorol. Soc.*, 93, 845–859, doi:10.1175/BAMS-D-11-00145.1, 2012.
- Giorgetta, M. A., Jungclaus, J., Reick, C. H., Legutke, S., Bader, J., Böttinger, M., Brovkin, V., Crueger, T., Esch, M., Fieg, K., Glushak, K., Gayler, V., Haak, H., Hollweg, H.-D., Ilyina, T., Kinne, S., Kornbluh, L., Matei, D., Mauritsen, T., Mikolajewicz, U., Mueller, W., Notz, D., Pithan, F., Raddatz, T., Rast, S., Redler, R., Roeckner, E., Schmidt, H., Schnur, R., Segschneider, J., Six, K. D., Stockhause, M., Timmreck, C., Wegner, J., Widmann, H., Wieners, K.-H., Claussen, M., Marotzke, J., and Stevens, B.: Climate and carbon cycle changes from 1850 to 2100 in MPI-ESM simulations for the coupled model intercomparison project phase 5, *J. Adv. Model. Earth Syst.*, 5, 572–597, doi:10.1002/jame.20038, 2013.
- Graf, H.-F., Kirchner, I., Robock, A., and Schult, I.: Pinatubo eruption winter climate effects: model versus observations, *Clim. Dynam.*, 9, 81–93, doi:10.1007/BF00210011, 1993.
- Graf, H.-F., Li, Q., and Giorgetta, M. A.: Volcanic effects on climate: revisiting the mechanisms, *Atmos. Chem. Phys.*, 7, 4503–4511, doi:10.5194/acp-7-4503-2007, 2007.
- Kirchner, I., Stenchikov, G. L., Graf, H.-F., Robock, A., and Antuña, J. C.: Climate model simulation of winter warming and summer cooling following the 1991 Mount Pinatubo volcanic eruption, *J. Geophys. Res.*, 104, 19039–19055, doi:10.1029/1999JD900213, 1999.
- Kodera, K.: Influence of volcanic eruptions on the troposphere through stratospheric dynamical processes in the Northern Hemisphere winter, *J. Geophys. Res.*, 99, D01273, doi:10.1029/93JD02731, 1994.
- Kodera, K.: On the origin and nature of the interannual variability of the winter stratospheric circulation in the Northern Hemisphere, *J. Geophys. Res.*, 100, 14077, doi:10.1029/95JD01172, 1995.
- Labitzke, K. and McCormick, M. P.: Stratospheric temperature increases due to Pinatubo aerosols, *Geophys. Res. Lett.*, 19, 207–210, doi:10.1029/91GL02940, 1992.
- Labitzke, K. and van Loon, H.: The Southern Oscillation. Part IX: The influence of volcanic eruptions on the Southern Oscillation in the stratosphere, *J. Climate*, 2, 1223–1226, doi:10.1175/1520-0442(1989)002<1223:TSOPIT>2.0.CO;2, 1989.
- Marshall, A. G., Scaife, A. A., and Ineson, S.: Enhanced seasonal prediction of European winter warming following volcanic eruptions, *J. Climate*, 22, 6168, doi:10.1175/2009JCLI3145.1, 2009.
- McLandress, C. and Shepherd, T. G.: Simulated anthropogenic changes in the Brewer–Dobson circulation, including its extension to high latitudes, *J. Climate*, 22, 1516–1540, doi:10.1175/2008JCLI2679.1, 2009.
- Muthers, S., Anet, J. G., Raible, C. C., Brönnimann, S., Rozanov, E., Arfeuille, F., Peter, T., Shapiro, A. I., Beer, J., Steinhilber, F., Bruhnara, Y., and Schmutz, W.: Northern hemispheric winter warming pattern after tropical volcanic eruptions: sensitivity to the ozone climatology, *J. Geophys. Res.-Atmos.*, 119, 1340–1355, doi:10.1002/2013JD020138, 2014.
- Newman, P. A. and Rosenfield, J. E.: Stratospheric thermal damping times, *Geophys. Res. Lett.*, 24, 433–436, doi:10.1029/96GL03720, 1997.
- Newman, P. A., Nash, E. R., and Rosenfield, J. E.: What controls the temperature of the Arctic stratosphere during the spring?, *J. Geophys. Res.*, 106, 19999, doi:10.1029/2000JD000061, 2001.
- Perlwitz, J. and Graf, H.-F.: The statistical connection between tropospheric and stratospheric circulation of the Northern Hemisphere in winter, *J. Climate*, 8, 2281–2295, doi:10.1175/1520-0442(1995)008<2281:TSCBTA>2.0.CO;2, 1995.
- Pitari, G.: A numerical study of the possible perturbation of stratospheric dynamics due to Pinatubo aerosols – implications for tracer transport, *J. Atmos. Sci.*, 50, 2443–2461, doi:10.1175/1520-0469(1993)050<2443:ANSOTP>2.0.CO;2, 1993.
- Pitari, G. and Mancini, E.: Short-term climatic impact of the 1991 volcanic eruption of Mt. Pinatubo and effects on atmospheric tracers, *Nat. Hazards Earth Syst. Sci.*, 2, 91–108, doi:10.5194/nhess-2-91-2002, 2002.
- Poberaj, C. S., Staehelin, J., and Brunner, D.: Missing stratospheric ozone decrease at Southern Hemisphere middle latitudes after

- Mt. Pinatubo: a dynamical perspective, *J. Atmos. Sci.*, 68, 1922–1945, doi:10.1175/JAS-D-10-05004.1, 2011.
- Polvani, L. M. and Waugh, D. W.: Upward wave activity flux as a precursor to extreme stratospheric events and subsequent anomalous surface weather regimes, *J. Climate*, 17, 3548–3554, doi:10.1175/1520-0442(2004)017<3548:UWAFAA>2.0.CO;2, 2004.
- Robock, A.: Volcanic eruptions and climate, *Rev. Geophys.*, 38, 191–219, doi:10.1029/1998RG000054, 2000.
- Robock, A. and Mao, J.: Winter warming from large volcanic eruptions, *Geophys. Res. Lett.*, 19, 2405, doi:10.1029/92GL02627, 1992.
- Rozanov, E. V.: Climate/chemistry effects of the Pinatubo volcanic eruption simulated by the UIUC stratosphere/troposphere GCM with interactive photochemistry, *J. Geophys. Res.*, 107, 4594, doi:10.1029/2001JD000974, 2002.
- Russell, P. B., Livingston, J. M., Pueschel, R. F., Bauman, J. J., Pollack, J. B., Brooks, S. L., Hamill, P., Thomason, L. W., Stowe, L. L., Deshler, T., Dutton, E. G., and Bergstrom, R. W.: Global to microscale evolution of the Pinatubo volcanic aerosol derived from diverse measurements and analyses, *J. Geophys. Res.*, 101, 18745–18763, doi:10.1029/96JD01162, 1996.
- Sato, M., Hansen, J. E., McCormick, M. P., and Pollack, J. B.: Stratospheric aerosol optical depths, 1850–1990, *J. Geophys. Res.*, 98, 22987–22994, doi:10.1029/93JD02553, 1993.
- Schmidt, H., Rast, S., Bunzel, F., Esch, M., Giorgetta, M., Kinne, S., Krismer, T., Stenchikov, G., Timmreck, C., Tomassini, L., and Walz, M.: Response of the middle atmosphere to anthropogenic and natural forcings in the CMIP5 simulations with the Max Planck Institute Earth system model, *J. Adv. Model. Earth Syst.*, 5, 98–116, doi:10.1002/jame.20014, 2013.
- Seviour, W. J. M., Butchart, N., and Hardiman, S. C.: The Brewer–Dobson circulation inferred from ERA-Interim, *Q. J. Roy. Meteor. Soc.*, 138, 878–888, doi:10.1002/qj.966, 2012.
- Shepherd, T. G. and McLandress, C.: A robust mechanism for strengthening of the Brewer–Dobson circulation in response to climate change: critical-layer control of subtropical wave breaking, *J. Atmos. Sci.*, 68, 784–797, doi:10.1175/2010JAS3608.1, 2011.
- Shindell, D. T.: Dynamic winter climate response to large tropical volcanic eruptions since 1600, *J. Geophys. Res.*, 109, D05104, doi:10.1029/2003JD004151, 2004.
- Shindell, D. T., Schmidt, G. A., Miller, R. L., and Rind, D.: Northern Hemisphere winter climate response to greenhouse gas, ozone, solar, and volcanic forcing, *J. Geophys. Res.*, 106, D07193, doi:10.1029/2000JD900547, 2001.
- Stenchikov, G.: Arctic oscillation response to the 1991 Mount Pinatubo eruption: effects of volcanic aerosols and ozone depletion, *J. Geophys. Res.*, 107, 4803, doi:10.1029/2002JD002090, 2002.
- Stenchikov, G., Kirchner, I., Robock, A., Graf, H.-F., Antuña, J. C., Grainger, R. G., Lambert, A., and Thomason, L.: Radiative forcing from the 1991 Mount Pinatubo volcanic eruption, *J. Geophys. Res.*, 103, 13837–13857, doi:10.1029/98JD00693, 1998.
- Stenchikov, G., Hamilton, K., Stouffer, R. J., Robock, A., Ramaswamy, V., Santer, B., and Graf, H.-F.: Arctic Oscillation response to volcanic eruptions in the IPCC AR4 climate models, *J. Geophys. Res.*, 111, D07107, doi:10.1029/2005JD006286, 2006.
- Thomason, L. W. and Peter, T. (Eds.): Assessment of Stratospheric Aerosol Properties (ASAP), SPARC Report No. 4, WCRP-124, WMO/TD-No. 1295, 2006.
- Timmreck, C., Lorenz, S. J., Crowley, T. J., Kinne, S., Raddatz, T. J., Thomas, M. A., and Jungclaus, J. H.: Limited temperature response to the very large AD 1258 volcanic eruption, *Geophys. Res. Lett.*, 36, L21708, doi:10.1029/2009GL040083, 2009.
- Timmreck, C., Graf, H.-F., Lorenz, S. J., Niemeier, U., Zanchettin, D., Matei, D., Jungclaus, J. H., and Crowley, T. J.: Aerosol size confines climate response to volcanic super-eruptions, *Geophys. Res. Lett.*, 37, L24705, doi:10.1029/2010GL045464, 2010.
- Tooney, M., Krüger, K., Niemeier, U., and Timmreck, C.: The influence of eruption season on the global aerosol evolution and radiative impact of tropical volcanic eruptions, *Atmos. Chem. Phys.*, 11, 12351–12367, doi:10.5194/acp-11-12351-2011, 2011.